Journal of Earth Science, *Vol. 33*, *No. 3*, *p. 770–777*, *June 2022* *ISSN 1674-487X*
Printed in China
https://doi.org/10.1007/s12583-021-1574-0

Thermal Conductivity and Thermal Diffusivity of Ferrosilite under High Temperature and High Pressure

Bo Feng[1, 2], **Xinzhuan Guo**[*1, 2]
1. *Key Laboratory for High-Temperature and High-Pressure Study of the Earth's Interior, Institute of Geochemistry, Chinese Academy of Sciences*, *Guiyang* 550081, *China*
2. *University of Chinese Academy of Sciences*, *Beijing* 100049, *China*
Bo Feng: https://orcid.org/0000-0002-6101-9034; Xinzhuan Guo: https://orcid.org/0000-0002-0916-5085

ABSTRACT: Orthopyroxene is an important constitutive mineral in the crust and the upper mantle. Its thermal properties play a key role in constructing the thermal structure of the crust and the upper mantle. In this study, we developed a new method to synthesize polycrystalline ferrosilite, one end-member of orthopyroxene, via the reaction of FeO + SiO_2 → $FeSiO_3$. We found that the *P-T* condition of 3 GPa and 1 273 K is suitable to synthesize dense ferrosilite samples with low porosity. We employed the transient plane-source method to investigate the thermal conductivity κ and thermal diffusivity *D* of synthetic ferrosilite at 1 GPa and 293–873 K, of which, $\kappa = 1.786 + 1.048 \times 10^3 T^{-1} - 9.269 \times 10^4 T^{-2}$ and $D = 0.424 + 0.223 \times 10^3 T^{-1} + 1.64 \times 10^4 T^{-2}$. Our results suggest phonon conduction should be the dominant mechanism at *P-T* conditions of interest since the thermal conductivity and the thermal diffusivity of ferrosilite both decrease with increasing temperature. The calculated heat capacity of ferrosilite at 1 GPa increases with temperature, which increases with increasing temperature with about 10% per 100 K (<500 K) and 4% per 100 K (>500 K). Iron content of an asteroid significantly influences its thermal evolution history and temperature distribution inside. It is expected that the mantle temperature of the Fe-rich asteroid will be higher and the Fe-rich asteroid's cooling history will be longer.
KEY WORDS: ferrosilite, high pressure, thermal conductivity, thermal diffusivity, synthesis.

0 INTRODUCTION

Pyroxene is considered to be one of the main constituent minerals in the upper mantle (Ringwood, 1975), which includes two subgroups of orthopyroxene and clinopyroxene. Ferrosilite ($FeSiO_3$) is one end-member of orthopyroxene. Enstatite ($MgSiO_3$) and ferrosilite can form ideal solid solution through the Mg-Fe substitution. Although the iron number [100 × Fe/(Fe + Mg)] of the shallower upper mantle is about 10 (Ono and Oganov, 2005; Gaul et al., 2000), not only in the deeper mantle where composition heterogeneity has been observed (Ringwood, 1991), but also in terrestrial planes whose Fe concentration is distinguished from that of the Earth, e.g., the Mars (Khan et al., 2018). The Fe concentration of some asteroids surface was also found to range from 49 to 70 (Sanchez et al., 2014; Sunshine et al., 2007). The iron content of orthopyroxenes could be different. It has been known that iron content greatly influences the physical properties of orthopyroxene (Zhang and Yoshino, 2016; Hofmeister, 2012; Stalder, 2004), and also influences the thermal conductivity and thermal diffusivity of olivine (Zhang Y Y et al., 2019). In order to illuminate iron content effect on the thermal conductivity and thermal diffusivity of orthopyroxene, it is necessary to survey the thermal properties of ferrosilite, which has not been reported ever before.

To synthesize ferrosilite, high-pressure and high-temperature technique is generally required. There are mainly two methods to synthetize ferrosilite: One method employed mixture of SiO_2, Fe_2O_3, Fe and 1 wt.% ultrapure water to synthesize ferrosilite between 1 000–1 200 ℃ at 3 GPa (Xu et al., 2020). The employment of water will inevitably inject hydrogen into the crystal structure of ferrosilite at high pressure, and may strongly affect the thermal properties of the minerals (Chang et al., 2017). Another method employed high-temperature gas flow furnace to synthesize fayalite firstly from mixture of Fe_2O_3 and SiO_2, and then employed high-pressure apparatus to synthesize ferrosilite finally from mixture of fayalite and SiO_2 at high temperatures (Kung and Li, 2014; Giuli et al., 2002; Akimoto et al., 1964; Lindsley et al., 1964). This method is relatively complicated and the stability field of ferrosilite is not well determined yet (Giuli et al., 2002; Lindsley et al., 1964; Bowen and Schairer, 1935). Therefore, it is necessary to develop the synthesis method to overcome the above disadvantages and define effects of pressure and temperature.

In this study, we directly synthesize well-sintered ferrosilite with low porosity using the mixture of FeO and SiO_2 under high pressure and high temperature. Via the high quality polycrystals, we measured the thermal conductivity (κ) and thermal diffusivity (*D*) of ferrosilite at 1 GPa and 293–873 K. Based on

*Corresponding author: gxzhuan@mail.gyig.ac.cn

Manuscript received August 21, 2021.
Manuscript accepted October 29, 2021.

Feng Bo, Guo Xinzhuan, 2022. Thermal Conductivity and Thermal Diffusivity of Ferrosilite under High Temperature and High Pressure. *Journal of Earth Science*, 33(3): 770–777. https://doi.org/10.1007/s12583-021-1574-0. http://en.earth-science.net

the present experimental data, we calculated the temperature distribution and the thermal evolution of the Fe-rich and Fe-poor asteroids.

1 EXPERIMENTAL METHOD

1.1 Experimental Instruments

A YJ-3000 multi-anvil apparatus, installed at the High-Temperature and High-Pressure Laboratory of the Institute of Geochemistry, Chinese Academy of Sciences, Guiyang, was used for synthetic experiments and thermal conductivity experiments. The pressure was calibrated from the phase transition of metallic bismuth (ambient temperature at 2.54 GPa) and halide melting experiment (Fu et al., 2019). The temperature is monitored by a K-type (NiCr-NiAl) thermocouple. The approximate errors of pressure and temperature estimation are 0.1 GPa and 0.5 K, respectively.

1.2 Synthesis of Ferrosilite

High-purity FeO powder with a grain size of about 10 μm together with SiO_2 powder (5 μm or 30 nm) were used the starting materials. The SiO_2 powder was baked at 1 273 K for 1 h in an oven before be weighted. The FeO and SiO_2 powders were weighed in equal mole ratio and well mixed in an agate mortar with acetone for 2 h. Then the mixture was dried in a vacuum container for 48 h. Finally, the mixture was compressed to a cylindrical shape by a hand-press and loaded into the sample capsule. Three materials, graphite, iron and molybdenum, were used as the sample capsules to investigate the effect of capsule on the synthesis of ferrosilite. The entire mixing and assembling process was operated in a transparent box filled by argon to prevent the oxidization of FeO. Under suitable conditions, ferrosilite can be synthesized through reaction

$$FeO + SiO_2 \rightarrow FeSiO_3 \quad (1)$$

Ferrosilite aggregates for thermal conductivity measurements were sintered with a Mo capsule in a multi-anvil apparatus. After recovery, disks with ~1.0-mm thickness and ~5.0-mm diameter were cored and used for subsequent measurements. The detailed experimental conditions and results are summarized in Table 1.

1.3 Ferrosilite Characterization

The micro-texture of the recovered sample was observed by a JSM-7800F scanning electron microscopy (SEM). The ferrosilite synthesized under the above conditions has been confirmed by the Raman technique (Fig. 1). The SEM observation shows that the sample contains nearly pure ferrosilite with a grain size of about 10 μm (Fig. 2a, YJ-123). The ferrosilite is dense and machinable with low porosity (Fig. 3), which is suitable for the measurements of thermal properties under high *P*-*T* conditions.

1.4 Thermophysical Properties Measurement

The measurement of thermophysical properties adopts the transient plane-source method (Osako et al., 2004; Dzhavadov, 1975). The assembly of thermal conductivity experiment is shown in Fig. 2. The detailed description for the cell assembly and method is basically the same as Zhang B H et al. (2019).

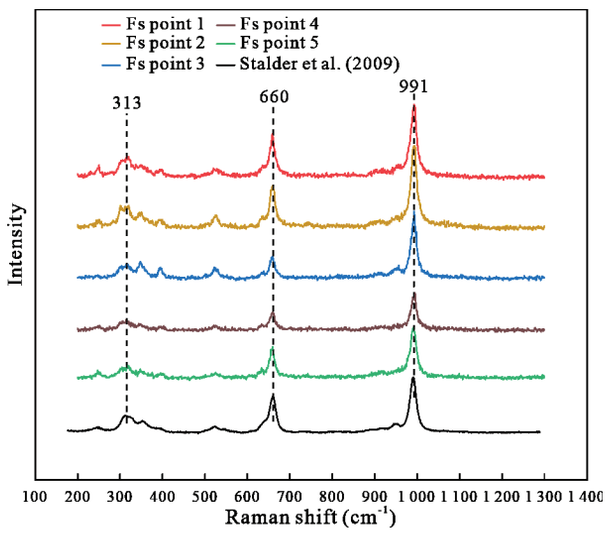

Figure 1. Raman spectra of synthetic ferrosilite. A laser beam with a wavelength of 514 nm was used to generate the Raman spectra of the sample. Totally 5 points were collected at 100 μm interval. Reference data are from Stalder et al. (2009).

Three disk samples with the same dimensions are piled face to face vertically at the center of the sample capsule. A planar impulse heater made of nickel was placed on one interface between the disks, while the thermocouple junction was set on the opposite interface. The sample was insulated from the graphite heater by MgO. Two nickel disks directly contacting with the sample were used as the heat sinks to satisfy the constant-temperature boundary.

During cooking, each pulse heating will cause the temperature fluctuation (ΔT) of the sample, which can be expressed as

$$\Delta T = A\sum_{n=1}^{\infty}\frac{1}{n^2}\sin\frac{n\pi}{3}\sin\frac{n\pi x}{d}\cdot \exp\left(-n^2B\tau\right)\left[\exp\left(n^2B\tau\right)-1\right]\ (t>\tau) \quad (2)$$

where x is the distance between impulse heater and thermocouple (m), d is the overall thickness of the three samples (m), τ is the pulse heating duration (s), and t is the time from the onset of heating (s). The parameters A and B are defined as follows

$$A=\frac{2Qd}{\pi^2\kappa S},\ B=\frac{\pi^2 D}{d^2} \quad (3)$$

where Q is the power used for impulse heating (W), S is the area of impulse heater (m^2), κ is the thermal conductivity ($W\cdot m^{-1}\cdot K^{-1}$), and D is the thermal diffusivity ($mm^2\cdot s^{-1}$). Since Eq. (2) for ΔT can reach a rapid convergence, a summation of n up to 15 should yield sufficiently accurate values (Yoneda et al., 2009; Osako et al., 2004), whose reliability has been confirmed by a finite element simulation (Yoneda et al., 2009).

The effect of heterogeneous temperature on results is negligible since with 8–16 W impulse power, the temperature disturbance across sample caused by impulse heating is only 3–6 K. Sample thickness and area during measurement was corrected according to the Birch-Murnaghan equation of state (EoS) (Hugh-Jones and Angel, 1997). Area change of impulse heater was corrected according to the equation $S_{(P,T)}/S_0=(V_{(P,T)}/V_0)^{2/3}$ used by Wang et al. (2014), where $S_{(P,T)}$, and $V_{(P,T)}$ are impulse heater ar-

Table 1 Experimental conditions and results for the synthesis of ferrosilite

No.	T (K)	P (GPa)	Duration (h)	Starting material	Capsule	Reaction products
Kawai-5	1 573	3	20	SiO_2 + FeO	Mo	Quench (Fs + FeO) + Qtz + Fe-Mo alloy
YJ-6	1 373	1.5	20	SiO_2 + FeO	Mo	FeO + Qtz
YJ-7	1 523	1.5	9	SiO_2 + FeO	Mo	Quench (Fa) + Qtz + Fe-Mo alloy
YJ-29	1 573	3	20	SiO_2 + FeO	Graphite	Quench (Fs + FeO) + Qtz
YJ-30	1 523	3	20	SiO_2 + FeO	Graphite	Quench (Fs + FeO) + Qtz
YJ-35	1 473	3	20	SiO_2 + FeO	Graphite	Quench (Fs + FeO) + Qtz
YJ-53	1 273	3	20	SiO_2 + FeO	Fe	Fa + Fs
YJ-55	1 273	2	20	SiO_2* + FeO	Graphite	Fs
YJ-56	1 273	3	20	SiO_2* + FeO	Graphite	Fs
YJ-58	1 373	2	15	SiO_2* + FeO	Graphite	Fa + Qtz
YJ-96	1 273	3	20	SiO_2 + FeO	Graphite	Fs + FeO + Qtz
YJ-170	1 273	1	20	SiO_2* + FeO	Graphite	Quench (Fa) + Qtz
YJ-123	1 273	3	2	Fs powder	Mo	Fs aggregates

*. Nano-scale SiO_2 was used; Fa. fayalite; Fs. ferrosilite; Qtz. quartz.

ea, and sample volume at high-pressure high-temperature conditions, respectively; and S_0, and V_0 are impulse heater area, and sample volume in ambient conditions, respectively. In the study, the total experimental systematic error is approximately 5% for both D and κ, which is mainly caused by errors associating with pulse heating power Q, sample thickness d, heating area S, and the least square fitting parameters of A and B in Eq. (3). Adopting the transient plane-source method, we measured κ and D of ferrosilite (YJ-123) at 1 GPa and 293–873 K (Table 2). In the experiment, the pressure was raised to the target value at 1 GPa/h, the temperature was raised at 20 K/min, and the heating interval was 100 K.

2 RESULTS AND DISCUSSION

2.1 Synthetic Ferrosilite

Under the conditions of different pressures and the same temperature, the run products are completely different. At 1 GPa and 1 273 K (Fig. 2c, YJ-170), the reaction products is mainly composed of fayalite and quartz; when the pressure is increased to 2–3 GPa, the reaction product is ferrosilite (Figs. 2b and 2e, YJ-56 and YJ-55). Obviously, as the pressure increases, ferrosilite can be better sintered under the same conditions. The molar volumes of fayalite, quartz, and ferrosilite are 46.41, 22.68, and 33.44 cm^3/mol, respectively. The sum of molar volumes of unit fayalite and quartz is greater than that of two unit ferrosilite (Table 3, modified from Lindsley et al., 1964). At higher pressures the reaction (1) will proceed towards the ferrosilite with a lower molar volume.

Under the same pressure and different temperatures, the run products are different. For example, at 2 GPa the run products are ferrosilite at 1 273 K (Fig. 2e, YJ-55) and Fa + Qtz at 1 373 K (Fig. 2f, YJ-58), respectively. Therefore, 2 GPa and 1 323 K may be the boundary conditions of the phase transition between Fs and Fa + Qtz. At constant pressure, higher temperature will increase the energy of the system, and enhance the vibration of the particles. Consequently, the reaction (1) will proceed towards fayalite and quartz with a larger molar volume (Newnham, 1975).

Table 2 Thermophysical properties of ferrosilite as a function of temperature at 1 GPa

T (K)	κ ($W \cdot m^{-1} \cdot K^{-1}$)	D ($mm^2 \cdot s^{-1}$)	c_p ($kJ \cdot kg^{-1} \cdot K^{-1}$)
292.24	4.275 (214)	1.383 (69)	0.785 (55)
374.05	4.001 (200)	1.120 (56)	0.906 (63)
476.72	3.637 (184)	0.975 (48)	0.947 (66)
573.86	3.224 (114)	0.870 (44)	0.941 (66)
674.35	3.098 (161)	0.788 (39)	0.997 (70)
774.02	2.946 (147)	0.728 (36)	1.027 (72)
875.41	2.965 (148)	0.704 (35)	1.069 (75)

Table 3 Molar volume of mineral aggregate (modified after Lindsley et al., 1964)

Aggregate with 2 $FeSiO_3$ components	Molar volume (cm^3/mol)
1 Fayalite + 1 quartz	69.09
1 Fayalite + 1 coesite	67.16
2 Ferrosilite	66.88

SiO_2 with nanometer grain size is more efficient than micrometer grain size in synthesizing ferrosilite due to the low reaction dynamics of SiO_2. To facilitate the reaction $Fe_2O_3 + Fe + 3SiO_2 = 3FeSiO_3$, Xu et al. (2020) added 1 wt.% water to the starting materials, which inevitably cause the contamination of sample by hydrogen. By reducing the grain size of SiO_2, ferrosilite can be easily synthesized with high quality. Among the three types of capsules, graphite, Fe, and Mo, the graphite capsule can provide a reducing environment for synthesis experiments and does not react with the starting materials. In summary, the ideal conditions for synthesizing ferrosilite are 3 GPa, 1 273 K, nano-scale SiO_2 as the starting material, and graphite as the sample capsule.

High porosity will significantly reduce the κ and D of polycrystalline samples (Xiong et al., 2020). In addition, high porosity of the sample will cause the difficulty in machining, larger deformation of the sample under high temperature and high pressure, larger temperature gradient, lower signal quality,

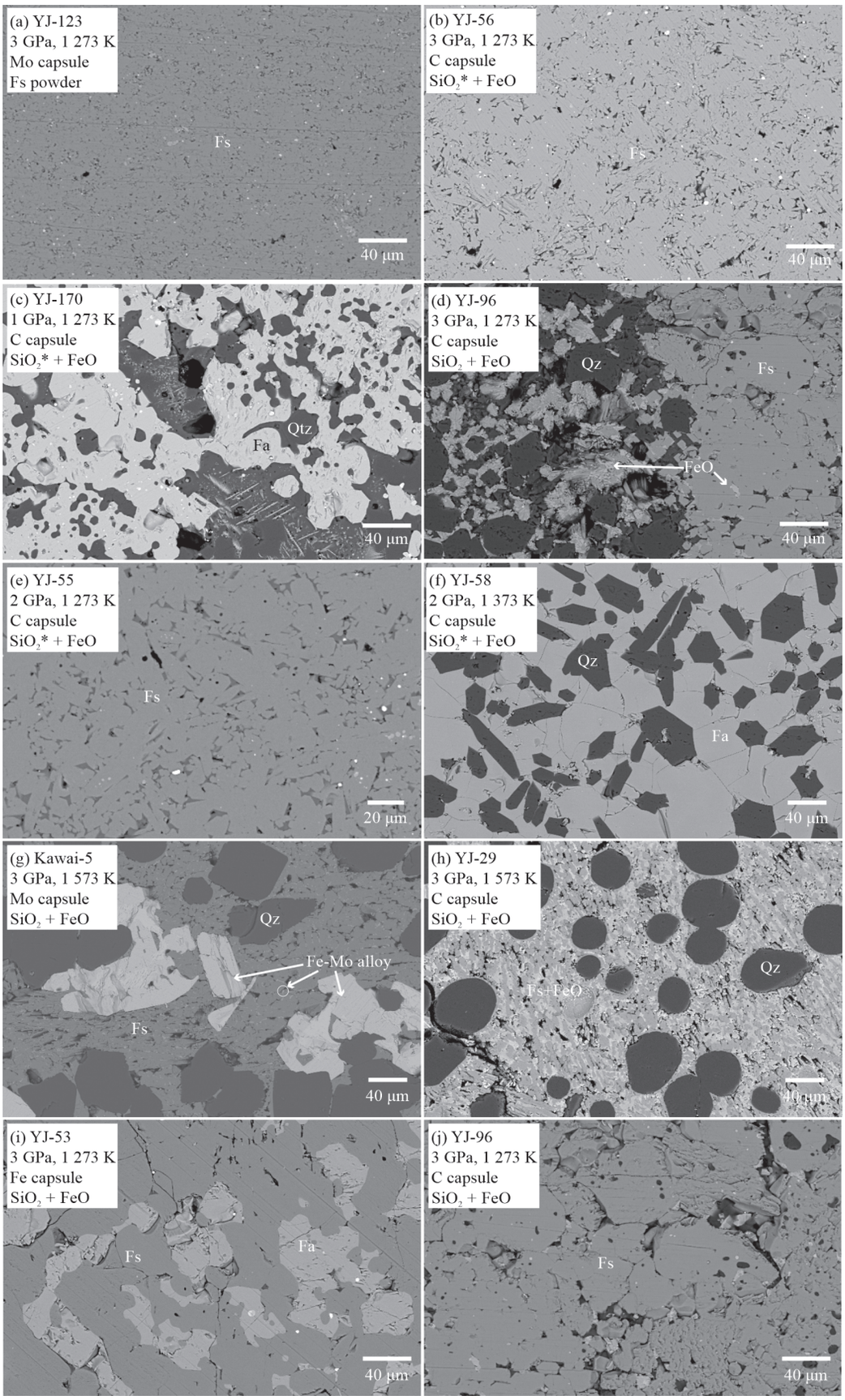

Figure 2. Back-scattered images of the recovered samples. The images of (a) synthetic ferrosilite; (b) and (e) synthetic samples under different pressures; (c), (e) and (f) synthetic samples at different temperatures; (b) and (d) the images of synthetic samples using micro-scale SiO_2 and nano-scale as the starting materials, respectively; (g), (h), (i) and (j) the images of synthetic samples using different capsules.

and larger fitting error of the data. In order to reduce the effect of the porosity on the *in-situ* measurements of the intrinsic κ and D of polycrystalline ferrosilite, the porosity of the sample should be as low as possible. We measured the κ and D of YJ-123 sample (Fig. 2a) synthesized at 3 GPa and 1 273 K using graphite as the sample capsule and nano-scale SiO_2 as the starting material.

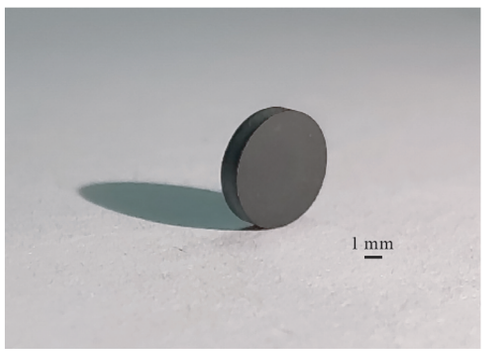

Figure 3. Ferrosilite sample with a diameter of 5 mm and a thickness of 1 mm.

2.2 Thermal Conductivity and Thermal Diffusivity

Figure 5 shows the signal of thermal disturbance generated by one single pulse heating (100 ms, 12 V). It clearly demonstrates the temperature change caused by the heat conduction of the sample. Using equations (2) and (3) to fit the thermal disturbance signal, we can obtain the thermal conductivity and thermal diffusion coefficient of ferrosilite at different temperatures. The fitting errors of parameters A and B are 1.26% and 1.92%, respectively. The relationship between the κ and D and the temperature can be expressed by the empirical formulas

$$\kappa = a_0 + a_1 T^{-1} + a_2 T^{-2} \quad (4)$$

$$D = b_0 + b_1 T^{-1} + b_2 T^{-2} \quad (5)$$

where a_0, a_1, a_2, b_0, b_1 and b_2 are the constants which we could obtained from non-linear least square fitting. The fitting results yield $a_0 = 1.786$, $a_1 = 1.048 \times 10^3$, $a_2 = -9.269 \times 10^4$, $b_0 = 0.424$, $b_1 = 0.223 \times 10^3$ and $b_2 = 1.640 \times 10^4$ (Table 4). Both the thermal conductivity and the thermal diffusivity decrease with increasing temperature, indicating the phonon conduction may be the dominant mechanism.

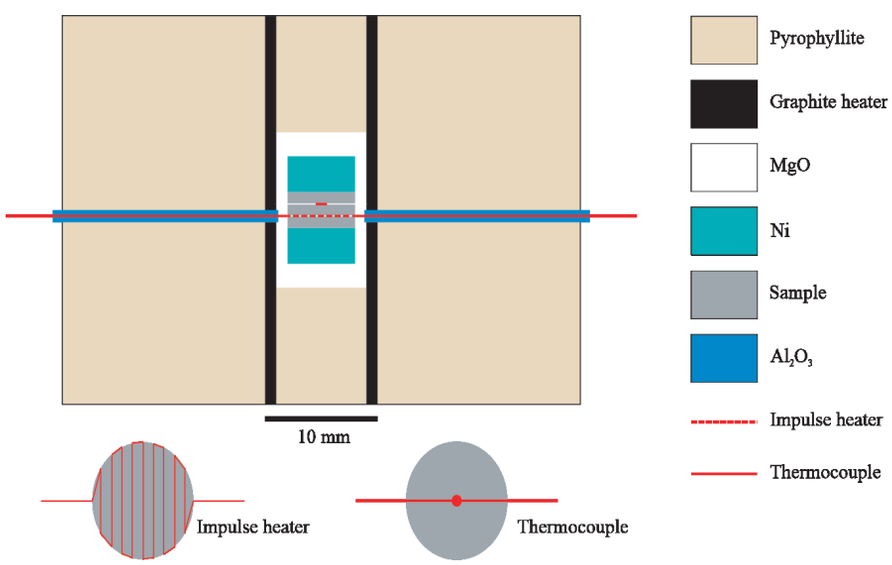

Figure 4. Schematic diagram of the cell assembly for the thermal properties measurements.

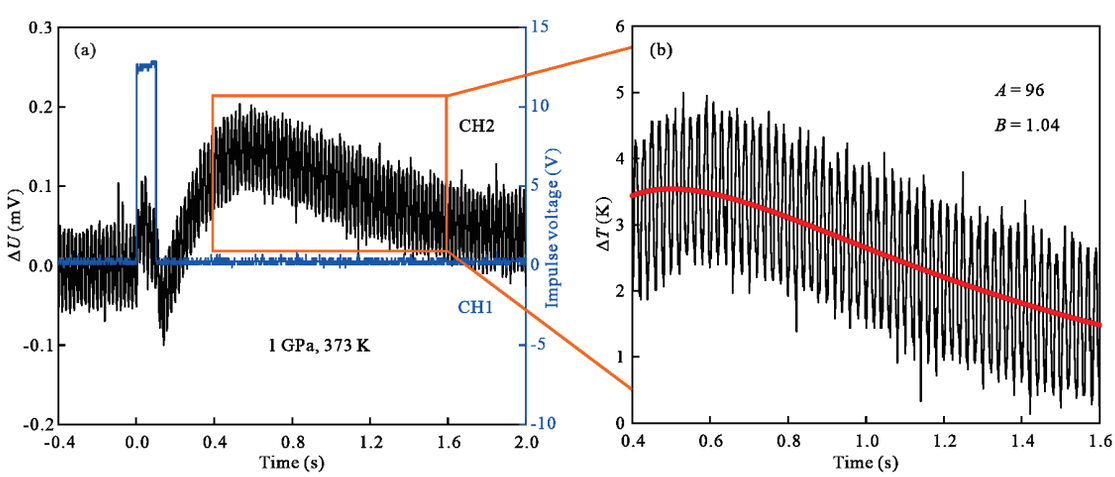

Figure 5. The records of oscilloscope of ferrosilite. (a) CH1 and CH2 are the signals of the inpulse heater and the thermocouple; (b) the amplified signals.

Table 4 Coefficient fitting for thermal conductivity and thermal diffusivity as a function of temperature

$\kappa(T) = a_0 + a_1T^{-1} + a_2T^{-2}$			
a_0 (W·m^{-1}·K^{-1})	a_1 (W·m^{-1})	a_2 (W·m^{-1}·K)	R^2
1.786	1.048×10^3	-9.269×10^4	0.980
$D(T) = b_0 + b_1T^{-1} + b_2T^{-2}$			
b_0 (mm^2·s^{-1})	b_1 (mm^2·s^{-1}·K)	b_2 (mm^2·s^{-1}·K^2)	R^2
0.424	0.223×10^3	1.640×10^4	0.998

Since there is no literature data of κ and D of ferrosilite, we compare the result of this study with natural enstatite En99 (Hofmeister, 2012), En98 (Hunt et al., 2011) and synthesized olivine, Fo and Fa (Zhang Y Y et al., 2019) (Figs. 6a and 6b). Thermal conductivity and thermal diffusivity of these samples all decrease with increasing temperature at constant pressure. Thermal conductivity of En99 reported by Hofmeister (2012) is higher than that of ferrosilite at 1 GPa and temperatures lower than 500 K. Thermal diffusivity of En99 at 1 atm is in agreement with that of ferrosilite at 1 GPa. However, the thermal diffusivities of En98 at 4 and 6 GPa (Hunt et al., 2011) are much higher than that of En99 at 1 atm (Fig. 6b), indicating a strong effect of pressure on the thermal diffusivity. At temperatures higher than 500 K, κ and D of ferrosilite and En99 become similar. The relatively large difference between this study and Hofmeister (2012) at low temperatures are similar to that of olivine. In the previous study of Zhang Y Y et al. (2019), the κ and D of forsterite are much larger than those of olivine with Fo number smaller than 90 at low temperatures. The pressure dependence of κ and D of forsterite and fayalite [$(\partial\kappa)/\partial P$, $(\partial D)/\partial P$] are 0.289, 0.122 and 0.064, 0.027, respectively (Zhang Y Y et al., 2019). The pressure has a greater effect on forsterite than fayalite.

The κ and D of the silicate minerals increase with increasing pressure (Hofmeister, 2007; Gibert et al., 2003), and decrease with increasing temperature and iron content (Zhang Y Y et al., 2019; Hofmeister and Pertermann, 2008; Schatz and Simmons, 1972). Combining the effects of pressure and iron content on the κ and D, the results of this study are reasonable.

2.3 Heat Capacity

Thermal conductivity κ and thermal diffusivity D of ferrosilite are determined simultaneously using present method, the heat capacity (c_p) can be calculated using the formula as follow (Clauser, 2011)

$$c_p = \frac{\kappa}{D\rho} \tag{6}$$

where ρ is the density, with that obtained by calorimetric measurements. Figure 6c shows the temperature dependence of the heat capacity (c_p) of ferrosilite at 1 GPa and the comparison between present results with previous ones (Saxena and Shen, 1992). The calculated heat capacity of ferrosilite at 1 GPa increases with temperature with about 10% per 100 K (<500 K) and 4% per 100 K (>500 K). The pressure dependence of the specific heat capacity of ferrosilite is about 10% per GPa, which is larger than that of omphacite, diopside and jadeite (Wang et al., 2014). However, according to error transfer, the errors attached to the calculated specific heat capacity data points are about 7% for ferrosilite. Therefore, the difference of the heat capacity between this study and calorimetric measurements is acceptable.

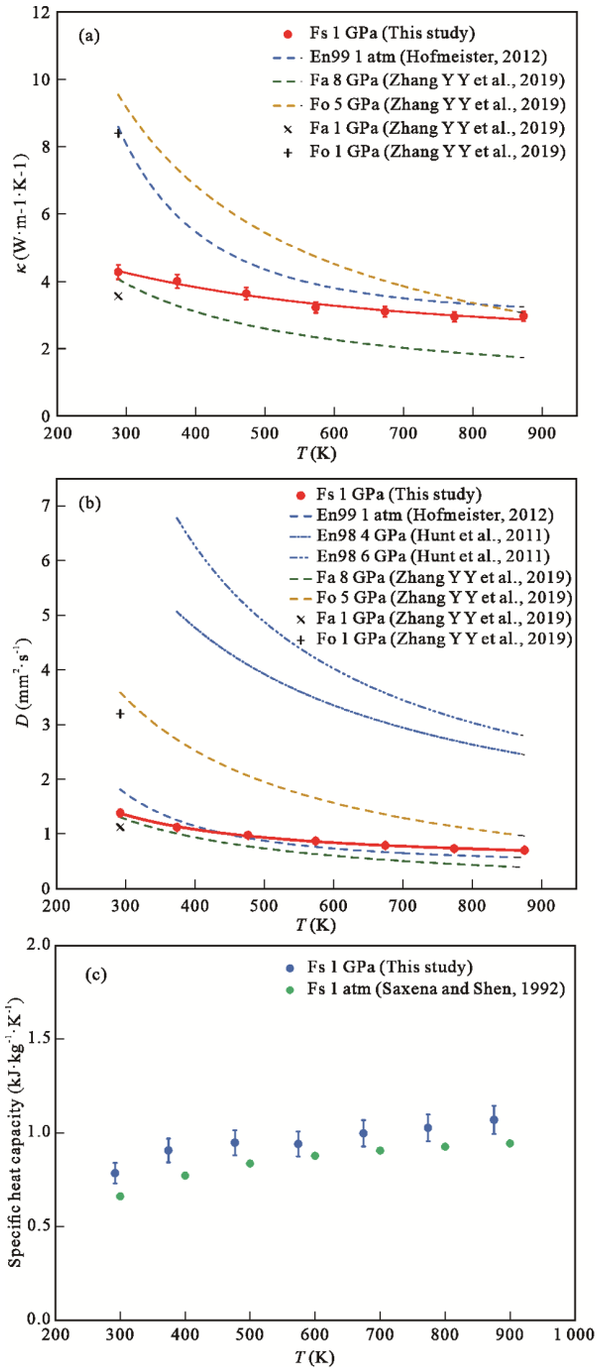

Figure 6. The temperature dependence on the thermal physical properties of ferrosilite and the comparison with previous studies. (a) The thermal conductivity of ferrosilite at 293–873 K. Reference data are from En99 (Hofmeister, 2012) and Fa, Fo (Zhang Y Y et al., 2019). (b) The thermal diffusivity of ferrosilite at 293–873 K. Reference data are from En99, En98 (Hofmeister, 2012; Hunt et al., 2011) and Fa, Fo (Zhang Y Y et al., 2019). (c) Calculated heat capacity of ferrosilite at 1 GPa and measured one at 1 atm by calorimetric method (Saxena and Shen, 1992).

2.4 Planetary Applications

The thermal history of asteroids plays an important role in understanding terrestrial planet formation. Zhang Y Y et al. (2019) survey the effect of Fe on the cooling history of asteroids. According to their results the cooling rate of asteroids decreases with increasing iron content. In their calibration, they used olivine to simulate the bulk composition. In this study, we used pyroxene instead of olivine to simulate the bulk composition. We used a simple heat conduction model of asteroids (Zhang Y Y et al., 2019). This model completely ignores other complex factors related to the thermal evolution of asteroids, such as the role of internal heat sources. At the same time, the model does not consider the influence of the shape of the asteroid. Asteroids consist of only a single phase, and only transfer heat through thermal conduction. The radius of the asteroid is 500 km. Initially, the temperature is homogeneously distributed inside the asteroid, with a temperature of 1 500 K. Based on the above assumptions, we use the software COMSOLTM to simulate the heat transfer process. We performed the simulation using constant thermal conductivity at room temperature, which maximizes the difference between different minerals.

Figure 7 show the temperature distribution inside the asteroids at 1 Gy and time-dependent temperature of the center point of the asteroids with constant thermal conductivity. The enstatite asteroid cools very quickly, and it has basically cooled within 1 Gy. The cooling of ferrosilite is slower than enstatite, and the temperature only drops by 66% at 1 Gy. The temperature between the internal and surface of the enstatite asteroid is less than 100 K, while the ferrosilite asteroid is greater than 500 K. This is basically consistent with the simulation results of olivine endmember minerals. Interestingly, the evolution results of the two asteroids composed of enstatite and forsterite, respectively, are basically the same, while the two asteroids composed of ferrosilite and fayalite, respectively, have a large gap. The temperature difference between the ferrosilite asteroid and the fayalite asteroid increases with time, and the difference is about 20% at 1 Gy. In order to quantitatively constrain the effect of iron content on the thermal evolution history of asteroids consisting of pyroxene, more experiments with variable iron contents should be conducted in the future. If we consider the asteroids, e.g., the Moon, the composition model consisting of both olivine and pyroxene should be used, in which case the calculated values of temperature distribution and time-dependent temperature should be intermediate between the values from olivine model and pyroxene model.

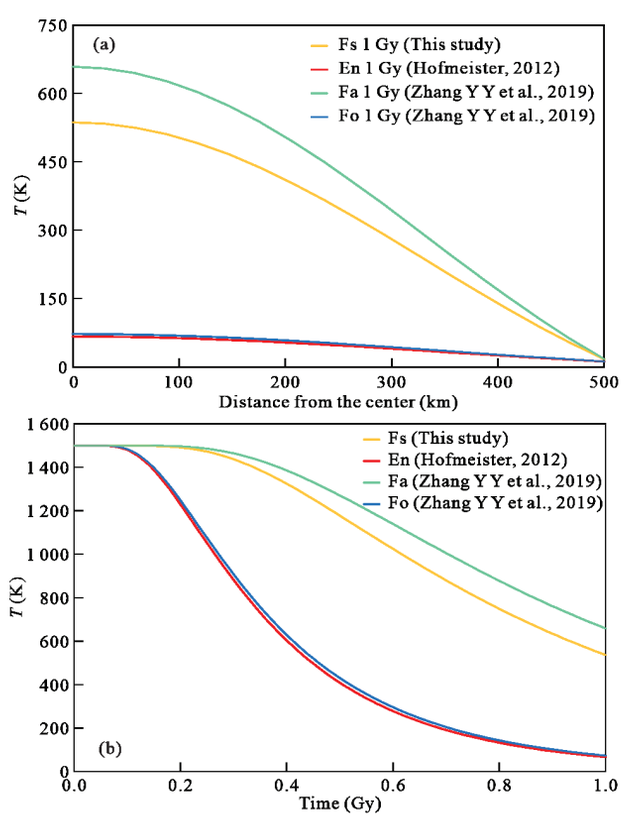

Figure 7. Temperature distribution inside the asteroids with different composition model. (a) Temperature distribution inside asteroids at 1 Gy. (b) Time-dependent temperature at the center of the asteroids with constant thermal conductivity. Reference data are from En99 at 1 atm (Hofmeister, 2012) and Fa, Fo at 1 GPa (Zhang Y Y et al., 2019).

3 CONCLUSION

Based on 12 synthesis experiments, we found that high temperature or low pressure is not benefit of the formation of ferrosilite. We used the sample synthesized for the *in-situ* measurements of the thermal conductivity and the thermal diffusivity. The thermal conductivity and the thermal diffusivity of ferrosilite are consistent with previous studies. The iron content of the bulk composition of asteroids strongly influences their cooling history and the temperature distribution. For Fe-rich asteroids, the mantle will be warmer. As a contrast, the heat will easily lose in the Fe-poor asteroid (e.g., Mercury).

ACKNOWLEDGMENTS

This study was supported by the CAS "Light of West China" Program (No. Y9CR026) and the National Natural Science Foundation of China (No. 442072051). The authors declare no competing financial interests. The final publication is available at Springer via https://doi.org/10.1007/s12583-021-1574-0.

REFERENCES CITED

Akimoto, S. I., Fujisawa, H., Katsura, T., 1964. Synthesis of $FeSiO_3$ Pyroxene (Ferrosilite) at High Pressures. *Proceedings of the Japan Academy*, 40(4): 272–275. https://doi.org/10.2183/pjab1945.40.272

Bowen, N. L., Schairer, J. F., 1935. The System MgO-FeO-SiO_2. *American Journal of Science*, 29(170): 151–217. https://doi.org/10.2475/ajs.s5-29.170.151

Chang, Y. Y., Hsieh, W. P., Tan, E., et al., 2017. Hydration-Reduced Lattice Thermal Conductivity of Olivine in Earth's Upper Mantle. *PNAS*, 114(16): 4078–4081. https://doi.org/10.1073/pnas.1616216114

Clauser, C., 2011. Thermal Storage and Transport Properties of Rocks, I: Heat Capacity and Latent Heat. Encyclopedia of Earth Sciences Series. Springer, Dordrecht. 1423–1431. https://doi.org/10.1007/978-90-481-8702-7_238

Dzhavadov, L. N., 1975. Measurement of Thermophysical Properties of Dielectrics under Pressure. *High Temperatures-High Pressures*, 7(1): 49–54

Fu, H. F., Zhang, B. H., Ge, J. H., et al., 2019. Thermal Diffusivity and Thermal Conductivity of Granitoids at 283–988 K and 0.3–1.5 GPa.

American Mineralogist, 104(11): 1533–1545. https://doi.org/10.2138/am-2019-7099

Gaul, O. F., Griffin, W. L., O'Reilly, S. Y., et al., 2000. Mapping Olivine Composition in the Lithospheric Mantle. *Earth and Planetary Science Letters*, 182(3/4): 223–235. https://doi.org/10.1016/s0012-821x(00)00243-0

Gibert, B., Seipold, U., Tommasi, A., et al., 2003. Thermal Diffusivity of Upper Mantle Rocks: Influence of Temperature, Pressure, and the Deformation Fabric. *Journal of Geophysical Research*: *Solid Earth*, 108(B8): 2359. https://doi.org/10.1029/2002jb002108

Giuli, G., Paris, E., Wu, Z. Y., et al., 2002. Fe and Mg Local Environment in the Synthetic Enstatite-Ferrosilite Join: An Experimental and Theoretical XANES and XRD Study. *European Journal of Mineralogy*, 14(2): 429–436. https://doi.org/10.1127/0935-1221/2002/0014-0429

Hofmeister, A. M., 2007. Pressure Dependence of Thermal Transport Properties. *PNAS*, 104(22): 9192–9197. https://doi.org/10.1073/pnas.0610734104

Hofmeister, A. M., 2012. Thermal Diffusivity of Orthopyroxenes and Proto-enstatite as a Function of Temperature and Chemical Composition. *European Journal of Mineralogy*, 24(4): 669–681. https://doi.org/10.1127/0935-1221/2012/0024-2204

Hofmeister, A. M., Pertermann, M., 2008. Thermal Diffusivity of Clinopyroxenes at Elevated Temperature. *European Journal of Mineralogy*, 20(4): 537–549. https://doi.org/10.1127/0935-1221/2008/0020-1814

Hugh-Jones, D. A., Angel, R. J., 1997. Effect of Ca^{2+} and Fe^{2+} on the Equation of State of $MgSiO_3$ Orthopyroxene. *Journal of Geophysical Research*: *Solid Earth*, 102(B6): 12333–12340. https://doi.org/10.1029/96jb03485

Hunt, S. A., Walker, A. M., McCormack, R. J., et al., 2011. The Effect of Pressure on Thermal Diffusivity in Pyroxenes. *Mineralogical Magazine*, 75(5): 2597–2610. https://doi.org/10.1180/minmag.2011.075.5.2597

Khan, A., Liebske, C., Rozel, A., et al., 2018. A Geophysical Perspective on the Bulk Composition of Mars. *Journal of Geophysical Research*: *Planets*, 123(2): 575–611. https://doi.org/10.1002/2017je005371

Kung, J., Li, B. S., 2014. Lattice Dynamic Behavior of Orthoferrosilite ($FeSiO_3$) Toward Phase Transition under Compression. *The Journal of Physical Chemistry C*, 118(23): 12410–12419. https://doi.org/10.1021/jp4112926

Lindsley, D. H., Davis, B. T., MacGregor, I. D., 1964. Ferrosilite ($FeSiO_3$): Synthesis at High Pressures and Temperatures. *Science*, 144(3614): 73–74. https://doi.org/10.1126/science.144.3614.73

Newnham, R. E., 1975. Structure-Property Relations. Springer-Verlag, Berlin. 60–64

Ono, S., Oganov, A. R., 2005. *In situ* Observations of Phase Transition between Perovskite and $CaIrO_3$-Type Phase in $MgSiO_3$ and Pyrolitic Mantle Composition. *Earth and Planetary Science Letters*, 236(3/4): 914–932. https://doi.org/10.1016/j.epsl.2005.06.001

Osako, M., Ito, E., Yoneda, A., 2004. Simultaneous Measurements of Thermal Conductivity and Thermal Diffusivity for Garnet and Olivine under High Pressure. *Physics of the Earth and Planetary Interiors*, 143/144: 311–320. https://doi.org/10.1016/j.pepi.2003.10.010

Ringwood, A. E., 1975. Composition and Petrology of the Earth's Mantle. McGraw-Hill, New York

Ringwood, A. E., 1991. Phase Transformations and Their Bearing on the Constitution and Dynamics of the Mantle. *Geochimica et Cosmochimica Acta*, 55(8): 2083–2110. https://doi.org/10.1016/0016-7037(91)90090-r

Sanchez, J. A., Reddy, V., Kelley, M. S., et al., 2014. Olivine-Dominated Asteroids: Mineralogy and Origin. *Icarus*, 228(2): 288–300. https://doi.org/10.1016/j.icarus.2013.10.006

Saxena, S. K., Shen, G. Y., 1992. Assessed Data on Heat Capacity, Thermal Expansion, and Compressibility for some Oxides and Silicates. *Journal of Geophysical Research*: *Solid Earth*, 97(B13): 19813–19825. https://doi.org/10.1029/92jb01555

Schatz, J. F., Simmons, G., 1972. Thermal Conductivity of Earth Materials at High Temperatures. *Journal of Geophysical Research*, 77(35): 6966–6983. https://doi.org/10.1029/jb077i035p06966

Stalder, R., 2004. Influence of Fe, Cr and Al on Hydrogen Incorporation in Orthopyroxene. *European Journal of Mineralogy*, 16(5): 703–711. https://doi.org/10.1127/0935-1221/2004/0016-0703

Stalder, R., Kronz, A., Schmidt, B. C., 2009. Raman Spectroscopy of Synthetic (Mg, Fe)SiO_3 Single Crystals: An Analytical Tool for Natural Orthopyroxenes. *European Journal of Mineralogy*, 21(1): 27–32. https://doi.org/10.1127/0935-1221/2009/0021-1846

Sunshine, J. M., Bus, S. J., Corrigan, C. M., et al., 2007. Olivine-Dominated Asteroids and Meteorites: Distinguishing Nebular and Igneous Histories. *Meteoritics & Planetary Science*, 42(2): 155–170. https://doi.org/10.1111/j.1945-5100.2007.tb00224.x

Wang, C., Yoneda, A., Osako, M., et al., 2014. Measurement of Thermal Conductivity of Omphacite, Jadeite, and Diopside up to 14 GPa and 1 000 K: Implication for the Role of Eclogite in Subduction Slab. *Journal of Geophysical Research*: *Solid Earth*, 119(8): 6277–6287. https://doi.org/10.1002/2014jb011208

Xiong, J., Lin, H. Y., Ding, H. S., et al., 2020. Investigation on Thermal Property Parameters Characteristics of Rocks and Its Influence Factors. *Natural Gas Industry B*, 7(3): 298–308. https://doi.org/10.1016/j.ngib.2020.04.001

Xu, J. G., Fan, D. W., Zhang, D. Z., et al., 2020. Phase Transition of Enstatite-Ferrosilite Solid Solutions at High Pressure and High Temperature: Constraints on Metastable Orthopyroxene in Cold Subduction. *Geophysical Research Letters*, 47(12): 1–10. https://doi.org/10.1029/2020gl087363

Yoneda, A., Osako, M., Ito, E., 2009. Heat Capacity Measurement under High Pressure: A Finite Element Method Assessment. *Physics of the Earth and Planetary Interiors*, 174(1/2/3/4): 309–314. https://doi.org/10.1016/j.pepi.2008.10.004

Zhang, B. H., Ge, J. H., Xiong, Z. L., et al., 2019. Effect of Water on the Thermal Properties of Olivine with Implications for Lunar Internal Temperature. *Journal of Geophysical Research*: *Planets*, 124(12): 3469–3481. https://doi.org/10.1029/2019je006194

Zhang, B. H., Yoshino, T., 2016. Effect of Temperature, Pressure and Iron Content on the Electrical Conductivity of Orthopyroxene. *Contributions to Mineralogy and Petrology*, 171(12): 1–12. https://doi.org/10.1007/s00410-016-1315-z

Zhang, Y. Y., Yoshino, T., Yoneda, A., et al., 2019. Effect of Iron Content on Thermal Conductivity of Olivine with Implications for Cooling History of Rocky Planets. *Earth and Planetary Science Letters*, 519: 109–119. https://doi.org/10.1016/j.epsl.2019.04.048